Article

Surfactant-Free Electroless Codeposition of Ni–P–MoS$_2$/Al$_2$O$_3$ Composite Coatings

Ping Liu [1,2,3,4,5,]*, **Yongwei Zhu** [1], **Qi Shen** [1], **Meifu Jin** [2], **Gaoyan Zhong** [2], **Zhiwei Hou** [4], **Xiao Zhao** [5], **Shuncai Wang** [5] **and Shoufeng Yang** [5,6]

1   Jiangsu Key Laboratory of Precision and Micro-Manufacturing Technology, Nanjing University of Aeronautics and Astronautics, Nanjing 210016, China; meeywzhu@nuaa.edu.cn (Y.Z.); sevenshenqi@163.com (Q.S.)
2   College of Engineering, Nanjing Agricultural University, Nanjing 210031, China; jinmeifu@njau.edu.cn (M.J.); gyzhong@njau.edu.cn (G.Z.)
3   Key Laboratory of Modern Agricultural Equipment and Technology, Ministry of Education/High-tech Key Laboratory of Agricultural Equipment & Intelligentization of Jiangsu Province, Jiangsu University, Zhenjiang 212013, China
4   Jiangsu Key Laboratory of Advanced Manufacturing Technology, Huaiyin Institute of Technology, Nanjing 223003, China; zw_hou66@163.com
5   Faculty of Engineering and Environment, University of Southampton, Southampton SO17 1BJ, UK; xiao.zhao@soton.ac.uk (X.Z.); wangs@soton.ac.uk (S.W.); s.yang@soton.ac.uk (S.Y.)
6   Production Engineering, Machine Design and Automation, Department of Mechanical Engineering, Katholieke Universiteit Leuven (KU Leuven), Leuven 3001, Belgium
*   Correspondence: liuping@njau.edu.cn; Tel.: +86-25-5860-6603

check for updates

Abstract: This paper presents the influence of an inorganic Al$_2$O$_3$ layer over MoS$_2$ particles on the tribological performance of electroless Ni–P–MoS$_2$/Al$_2$O$_3$ composite coatings fabricated without using surfactants. The Al$_2$O$_3$-coated MoS$_2$ particles were prepared by a heterogeneous nucleation process. The dry sliding tests of the composite coatings were tested against a WC ball. SEM was used to observe the surface morphology of particles, composite coatings, and worn surfaces. The results indicate that the coverage of an Al$_2$O$_3$ coating on MoS$_2$ particles significantly affects the surface morphology, frictional coefficient and wear loss of the composite coatings. The incorporation of Al$_2$O$_3$-coated MoS$_2$ particles with lower coverage (up to 7% of Al$_2$O$_3$) could obtain compact surface structure of composite coatings, which contribute to reduced wear loss. However, higher coverage would lead to loose surface structure of the composite coatings, and thus increase their wear loss.

Keywords: electroless composite coating; Al$_2$O$_3$-coated particles; MoS$_2$ particles; wear resistance; surfactant

1. Introduction

Electroless Nickel (EN) composite coatings containing submicro/nano-sized particles in a nickel matrix have received increasing attention in recent years [1–3]. The incorporation of solid particles into the matrix could remarkably improve the mechanical and physiochemical properties of composite coatings. For example, hard particles such as Al$_2$O$_3$ [4,5], SiC [6,7], SiO$_2$ [8], TiO$_2$ [9], and diamond [10] enhance the hardness and wear resistance of composite coatings. Solid lubricant particles such as MoS$_2$ [11,12], PTFE [13], and BN(h) [14] lower the frictional coefficient of composite coatings and consequently reduces wear loss. It was found that these superior properties highly rely upon a homogeneous distribution of particles in the coating matrix. However, most of the particles have

a strong tendency towards agglomeration in an EN solution [15–18]. To prevent agglomeration, surfactants are in particular added into the EN plating bath [19–21].

Surfactants (or surface active substances) are usually organic compounds that are amphiphilic. These lower the interfacial tension between particles and the EN solution by improving the wettability of particles [22]. These additives are very important in the incorporation of second phase particles, especially for water-repellent ones (e.g., MoS_2, PTFE) [23]. Without them, these hydrophobic particles would not be well immersed in the EN plating solution [22–24].

However, the adverse effects of using surfactants to produce composite coatings have recently been reported. Sudagar et al. [25] stated that the deposition of coating would be delayed (by as much 40 min) at the early stage due to the indirect contact of electrolytes with substrate caused by surfactant coverage. Zielinska et al. [26] discovered the coverage of surfactants on Ni ions and hypophosphite ions reduced the amounts of nickel and phosphorus in coatings by hampering the reduction process of nickel ions. The surfactant coverage on substrates also provided a barrier for the deposition of the coating, and thus decreased the deposition rate of composite coatings [27–31]. Mai et al. [32] argued that the introduction of additives weakens the interfacial bonding of particles and matrix, fading the properties of composite coatings. Furthermore, due to the complexity and selectivity of surfactants, numerous extra steps are required to identify suitable types and concentrations of surfactants for electroless composite plating [33–36]. Unfortunately, it is quite challenging to choose an appropriate surfactant for a specific plating configuration.

Recently, surface modification of inorganic coatings on particles has received considerable attention in several fields [37–39]. Our previous work [40] indicated that Al_2O_3 loading on the particles could improve the wettability of hydrophobic MoS_2 particles. As a result, we successfully incorporated the coated MoS_2 particles into a nickel matrix by the electroless plating method in the absence of surfactants [41–43], as shown in Figure 1. The resultant composite coatings showed improvements in wear property compared to those incorporated uncoated MoS_2 with aids of surfactants. These results indicated that the environmentally hazardous surfactants could be reduced or even excluded. In keeping with the nature of particles, an excessive coverage over particles is not expected. However, there are as yet only a few reports on the influence of particle coverage on composite coating performance.
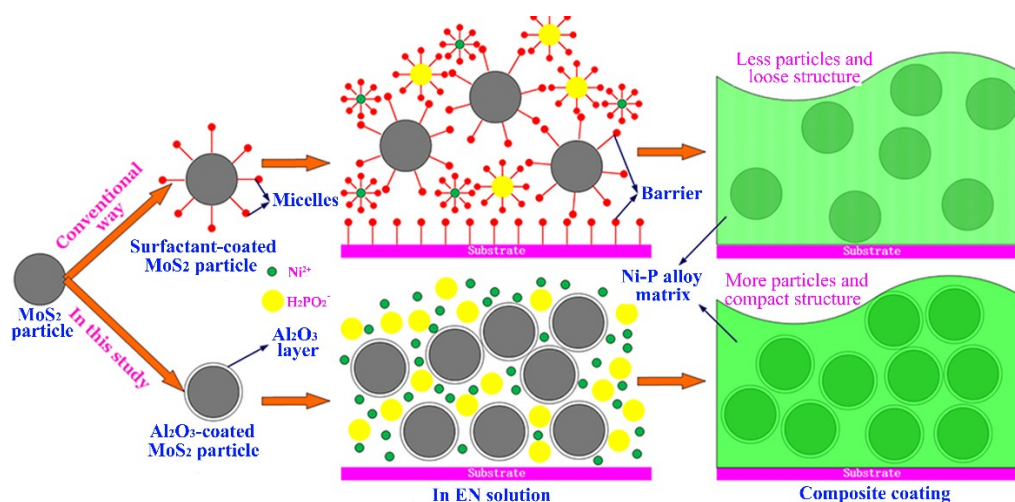
Figure 1. Diagram of the comparison between the codeposition of bare MoS_2 particles with surfactant and Al_2O_3-coated MoS_2 particles without surfactants into an electroless nickel matrix.

This work aims to evaluate the influence of particle coverage on the wear properties of the EN composite coatings. We prepared the Al_2O_3-coated MoS_2 particles with various coverages, and then used them to fabricate electroless composite coatings without using surfactants. The surface morphology, friction coefficient and wear loss of these composite coatings were investigated as well.

2. Materials and Methods

2.1. Preparation of Coated Particles

MoS$_2$ particles with an average particle size of Φ0.5 μm (supplied by Shanghai Haochem Company, Shanghai, China) were used to prepare the Al$_2$O$_3$-coated particles. In this process, the heterogeneous nucleation method was used (the detailed procedure may be found in our previous work [40]). Firstly, MoS$_2$ powder was etched 30 min with 20 wt %. H$_2$SO$_4$ solution at 80 °C to eliminate the oxide surface, and then cleaned with deionized (DI) water. Three grams of MoS$_2$ powder were added into 300 mL of NaOAc and HOAc-buffered solution with a pH of 4.5 to produce suspension. Al(OH)$_3$-coated MoS$_2$ particles were obtained by adding, via drops, 0.2 M Al(NO$_3$)$_3$ solution to the suspension, at an estimated rate of 0.05 mL/s. The reaction temperature was 60 °C. The pH was subjected to the addition of Al(NO$_3$)$_3$ solution, and kept at 4.5 $\pm$ 0.2. The loading of Al(OH)$_3$ on the particles was controlled by the reaction time. The reaction production was dried at 120 °C for 12 h, and subjected to dehydration in air at 350 °C for 2 h to produce Al$_2$O$_3$-coated particles. We designed a series of Al$_2$O$_3$-coated particles with amounts of coating ranging from 5% to 20% in increments of 5%, and a coating amount of 40% of the layer. However, we finally obtained the samples with loadings of 3%, 7%, 11%, 24% and 42%, respectively. The differences were attributed to the pH variability with the increased total volume of the suspension, which significantly affected the loading amount of Al(OH)$_3$.

The amounts of coating were determined by total water loss rate after being heated from 30 to 1200 °C at the heating rate of 20 K/min under Ar atmosphere condition. The decomposing reaction equation of Al(OH)$_3$ into Al$_2$O$_3$ and H$_2$O reveals that H$_2$O accounts for 34.6%, Al$_2$O$_3$ 65.4%. Given the total water loss rate λ, then the coverage of Al$_2$O$_3$ can be determined by the following equation (Equation (1)),

$$Al_2O_3 \text{ (wt \%)} = 65.4\%/34.6\% \; \lambda = 1.89 \; \lambda. \tag{1}$$

*2.2. Preparation of Ni–P Matrix Composite Coatings*

2.2.1. Substrate Preparation

Medium carbon steel specimens with the size of Φ 50 mm $\times$ 2 mm were used as substrates. Each substrate was polished using a 2000 grade abrasive paper and ultrasonically cleaned in acetone. All the substrates were degreased with an alkaline solution (Na$_2$CO$_3$ 30 g/L, NaOH 30 g/L, Na$_3$PO$_4$·12H$_2$O 10 g/L, Na$_2$SiO$_3$ 10 g/L, OP-10 2 mL/L) at 70–80 °C for 60 min, and then cleaned up with deionized water. After that, the substrates were activated in a 20 wt % H$_2$SO$_4$ aqueous solution for 90 s and rinsed with deionized water twice prior to plating.

2.2.2. Electroless Plating Bath and Operating Conditions

The commercial electroless plating solution (HK350 from Haibo Co. Ltd., Nanjing, China) was used to produce EN composite coatings. The composition of the plating solution mainly consists of NiSO$_4$ 25 g/L, NaH$_2$PO$_2$·H$_2$O 22 g/L, buffer agents, and stabilized agents. The plating process took place in a 500 mL thermostated vessel. For comparison, Ni–P–MoS$_2$ composite coating was fabricated as well. The pre-treated particles were first added to a separate portion of EN solution and dispersed by an ultrasonic cleaner for 20 min. In this step, it is easy to produce MoS$_2$ suspension for the coated particles without the aids of surfactant (see Figure 2a). However, the uncoated ones must use the surfactant of Cetyltrimethylammonium Bromide (CTAB) for this purpose (see Figure 2b). Then, the suspension was transferred to the main EN solution to produce a composite plating bath with a concentration of 1 g/L of particles. All the samples were pre-plated with an active layer of Ni–P alloy at 88 °C for 10 min before applying the composite coating plating. After that, the samples were placed vertically into the composite plating bath under these conditions: A pH of 5.0, a magnetic stirring rate of 700 rpm, and a duration of 90 min at 88 °C.
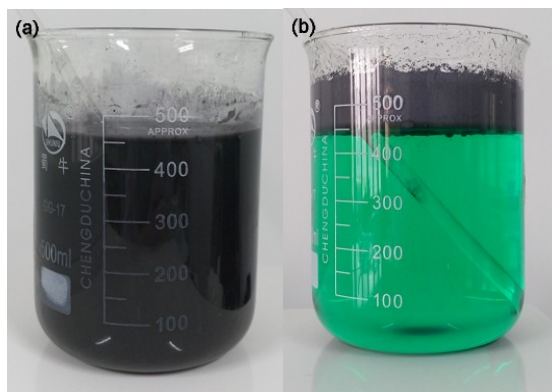
Figure 2. Particles suspension in EN plating bath of (**a**) Al_2O_3-coated MoS_2 particles, (**b**) pristine MoS_2 particles, respectively.

2.3. Post-Treatment of Electroless Coatings

All the as-prepared coatings have a similar coating thickness of 22–25 μm under the operation condition mentioned above. After preparation, these samples were first heated at 200 °C for 1 h to be dehydrogenated, and then heated at 400 °C for 1 h in air to reinforce the Ni–P matrix of composite coating [4].

2.4. SEM/EDS/XRD/LSCM Characterization

SEM (Hitachi S-4800, Tokyo, Japan) was used to observe the surface morphology of the coated MoS_2 particles and the composite coatings. EDS (Bruker EDS QUANTAX, Billerica, MA, USA) was employed to analyze the surface chemical composition of the coated particles. XRD (X'Pert PRO, Malvern Panalytical, Almelo, The Netherlands) with Cu Kα radiation was utilized to characterize the phase structure of the coated particles and composite coatings after heat treatment. The Laser-Scanning Confocal Microscope (LSCM, Olympus, OLS4100, Tokyo, Japan) was used to obtain the surface roughness of composite coatings.

2.5. Friction and Wear Tests

The friction and wear tests were carried out on a tribometer (CFT-1, Lanzhou, China) with a pin-on-disc contact configuration under dry sliding conditions. The composite coating specimens were used as rotating discs, and a tungsten carbide (WC) ball with a diameter of 6 mm was used as a fixed counterpart. For all the tests, the sliding velocity was fixed at 0.5 m/s with a contact radius of 12 mm, duration time of 4 h and normal load of 9.3 N. The worn scar was observed by using SEM (Hitachi S-4800) as well.

3. Results and Discussion

3.1. Al_2O_3-Coated MoS_2 Particles

Figure 3 illustrates the typical SEM morphologies of bare MoS_2 particles and the Al_2O_3-coated ones with the coverage of 7%, 24%, and 42%. The morphology of pristine MoS_2 particles is flat and smooth [40]. However, the surface of the coated particles became very rough, and the roughness varies with the amounts of Al_2O_3 loading. A lower amount of coating produces a partial cover on particles while a higher one produces an entire cover. It is worth mentioning that currently it is difficult to obtain a homogeneous coating layer over MoS_2 particles due to the strong hydrophobic feature of their pristine surfaces.
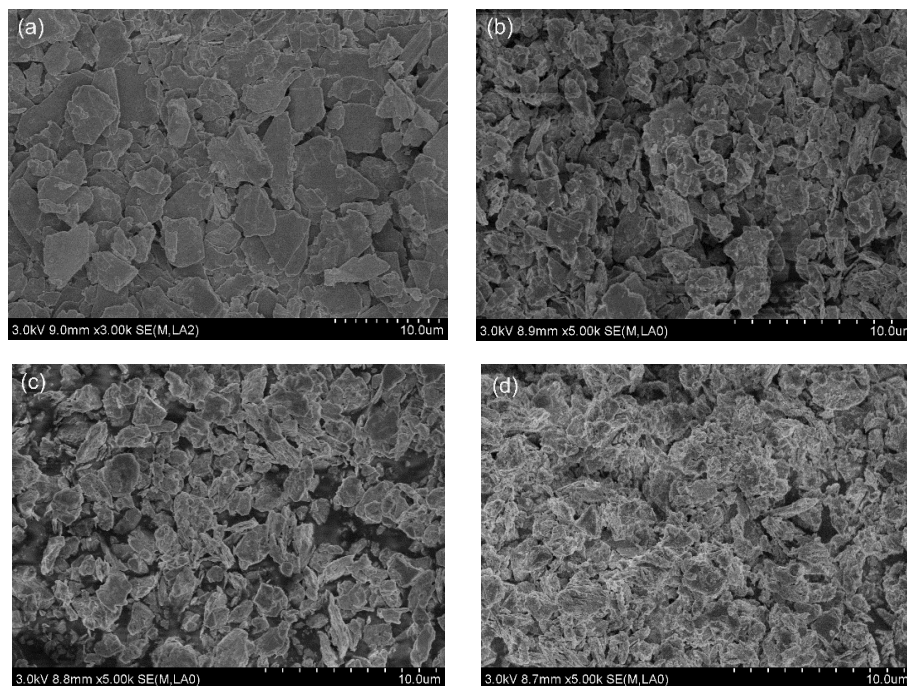
Figure 3. SEM morphology of MoS$_2$ particles (**a**) pristine particles [40], (**b**) Al$_2$O$_3$-coated particles with coverage of 7%, (**c**) Al$_2$O$_3$-coated particles with coverage of 24%, (**d**) Al$_2$O$_3$-coated particles with coverage of 42%, respectively. Adapted with permission from [40]. Copyright 2015 Elsevier.

The chemical compositions of the surface for the coated particles are determined by EDS and the structure is characterized by XRD, as discussed elsewhere [40]. EDS scanning over the surface of the as-coated particles with the coverage of 42% shows the Mo, S, O, and Al element is about 32 wt %, 16 wt %, 43 wt %, and 9 wt %, respectively. This result indicates the formation of aluminum hydroxide on the surface of particles. Figure 4 shows the XRD diffraction pattern of the coated particles with the coverage of 7% and 42% respectively after calcination at 350 °C. The XRD pattern reveals that the surface coating on particles is essentially an amorphous structure. Apart from MoS$_2$, no diffraction peak corresponding to alumina or aluminum hydroxide could be found. For comparison, the XRD diffraction pattern of Al(OH)$_3$ and Al$_2$O$_3$ are presented in our previous work [40]. The main reason is that the calcining temperature of 350 °C is insufficient to crystallize the as-amorphous structure of the aluminum hydroxide [44].
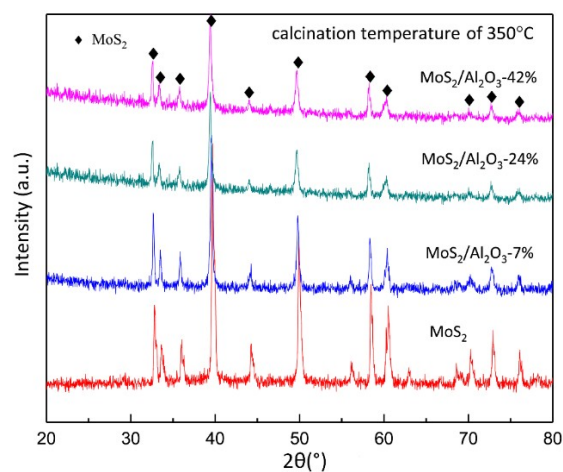
Figure 4. XRD pattern of MoS$_2$ particles and Al$_2$O$_3$-coated MoS$_2$ particles with loading of 7%, 24% and 42%, respectively, after calcining at 350 °C.

3.2. Ni–P Matrix Composite Coatings

Figure 5 shows the XRD patterns of the composite coatings containing Al_2O_3-coated MoS_2 particles with various coverage after heat treatment at 400 °C. The commercial electroless plating solution used in this study produces an amorphous Ni–P alloy matrix according to the indication of the manufacturer although the percentage of P cannot be evaluated. As a result, the transformation of the amorphous Ni–P matrix into Ni and Ni_3P phases took place after the heating treatment as most of the previous works have reported [4,45,46]. The phases transformation is independent of incorporation MoS_2 particles. This study reveals that the transformation is not affected whether the MoS_2 particles coated with Al_2O_3 or not.
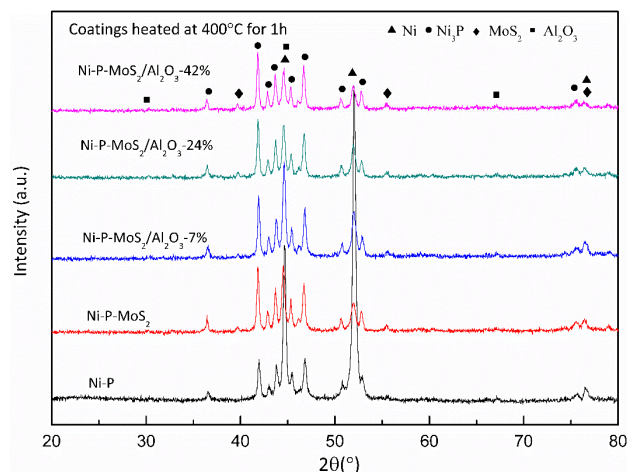
Figure 5. XRD patterns of EN composite coatings containing Al_2O_3-coated MoS_2 particles with various coverage after heat treatment at 400 °C.

The diffraction patterns corresponding to MoS_2 phase on all the composite coatings indicate that the MoS_2 particles have been successfully incorporated into the Ni–P matrix, have not involved in the transformation of the Ni–P matrix when heated. Very weak diffraction peaks of Al_2O_3 can be found for the composite coatings with coated MoS_2. The results are mainly attributed to a further dehydration and crystallization of aluminum hydroxide into alumina after the heating treatment at 400 °C as it exceeds the calcination temperature of 350 °C. However, the very small amount results in the weak diffraction intensity.

Figure 6 indicates the surface morphology and 3D images of EN composite coatings containing the coated MoS_2 particles with various Al_2O_3 coverage after heat treatment. The Ni–P–MoS_2 composite coating prepared using CTAB shows a spherical nodular structure, which is in line with most of the other literature [25,47,48]. The surface roughness S_a is 6.528 μm, as shown in Figure 6(a-2). A similar structure can also be seen on the surface of the composite coating with Al_2O_3 coverage of 3%. However, the latter shows a finer and homogeneous surface, whose surface roughness S_a is 3.135 μm, much less than the former. The increase of the coverage up to 7% could lead to a more compact surface structure of composite coating. The surface roughness decreased to S_a = 1.501 μm, as can be seen in Figure 6(c-2). The reason might be attributed to the role of Al_2O_3 loading on MoS_2 contributing to the fine grain size of the composite coatings. The Al_2O_3 loading could remarkably enhance the wettability of MoS_2 according to our previous findings [40]. This result indicates that less coverage of Al_2O_3 on particles could make it feasible to produce composite coatings without using surfactants.

The further increase of the coverage, however, would induce a reverse change of the surface morphology. The coatings show a loose surface structure with small nodules, large bumps and deep micropores, as shown in Figure 6e,f. The surface roughness also increases from S_a = 2.838 μm to S_a = 9.511 μm with the increase of coverage. This result might be attributed to the split of alumina from MoS_2 particles due to a large difference in elastic modulus between brittle Al_2O_3 and soft MoS_2.

The broken MoS$_2$ tends to form a film on the interface of plating bath, especially in the case of particles with high coverage. The MoS$_2$ film would hamper the escape of the hydrogen produced in the plating reaction, and result in the large bumps and deep micropores of the composite coating. On the other hand, the naked MoS$_2$ might be codeposited into the composite coating, as shown in Figure 6e,f (naked MoS$_2$). The incorporation of MoS$_2$ particles with highest loading of Al$_2$O$_3$ could lead to so very loose coating strucuture that the cross section of it could not obtained. Therefore, the higher coverage on particles is not recommended.
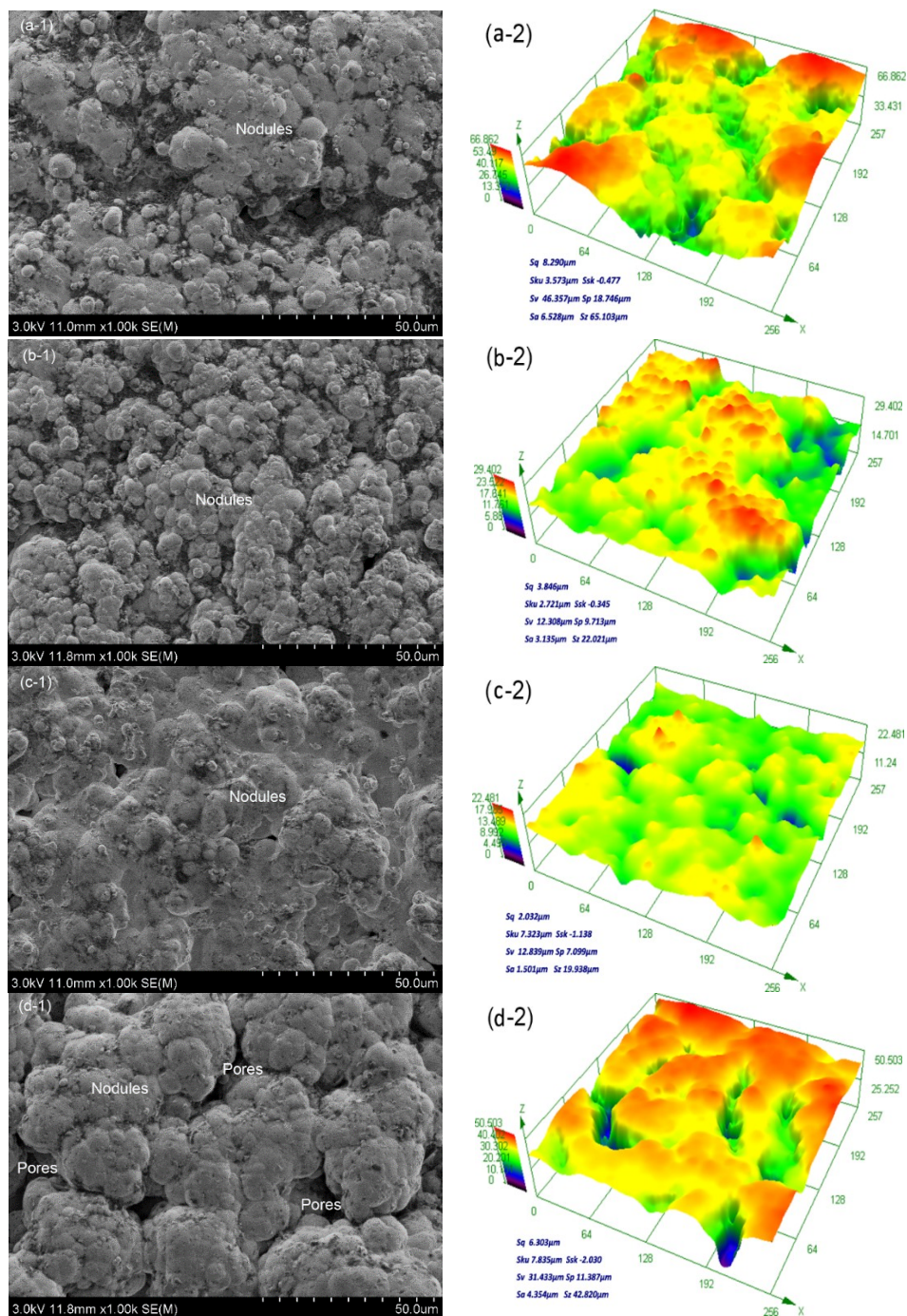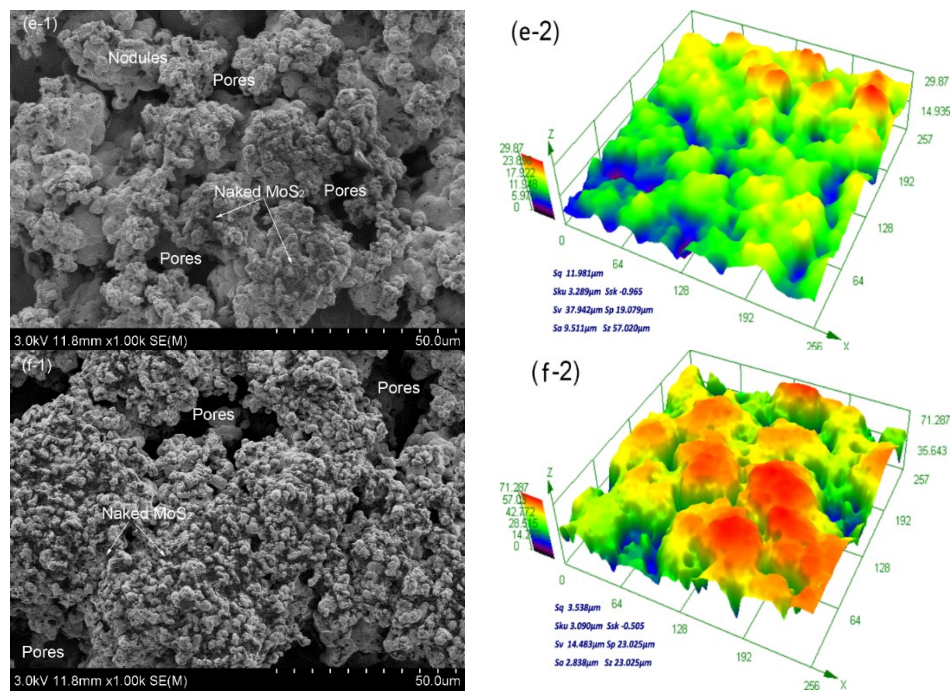

Figure 6. *Cont.*

Figure 6. SEM morphology and 3D images of EN composite coatings containing Al₂O₃-coated MoS₂ particles with various coverage after heat treatment at 400 °C: (**a**) 0%, (**b**) 3%, (**c**) 7%, (**d**) 11%, (**e**) 24%, (**f**) 42%, respectively.

3.3. Friction Coefficient

Figure 7 shows the evolution of friction coefficients for the EN composite coatings incorporating Al₂O₃-coated MoS₂ particles with various coverage while running against WC. Due to the very high hardness of its counterpart (WC), the Ni–P coating has a friction coefficient of approximately 0.6 at steady state after the running-in stage. Compared with the Ni–P alloy, the Ni–P–MoS₂ composite coating shows a significant decrease in the friction coefficient due to the lubricant effect of the MoS₂. However, its friction coefficient could not reach a steady state until it reached a sliding distance of up to 850 m, which is similar to that in the literature [49]. After that, its frictional coefficient tends to be stable at 0.4. This result is much smaller than that in the literature [11], which might be attributed to the submicro-sized particles used in this study.
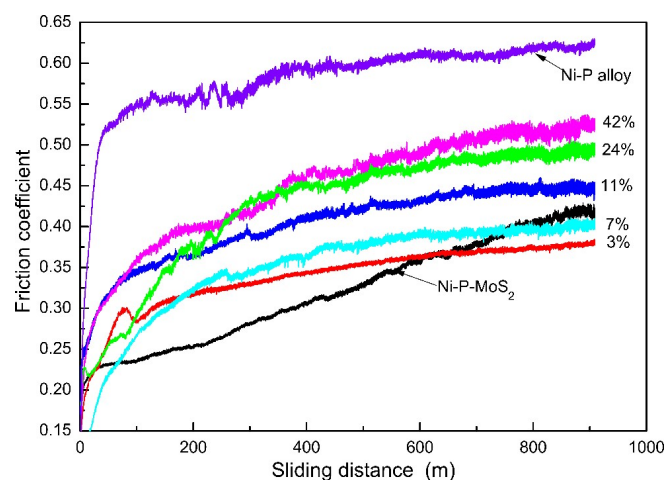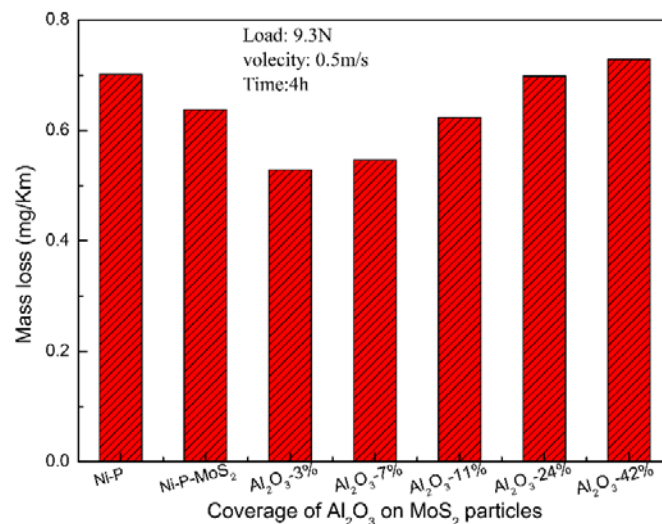

Figure 7. Friction coefficient of electroless composite coatings incorporating Al₂O₃-coated MoS₂ particles with various coverage.

The composite coatings with the coated MoS_2 indicate a relative steady evolution in the friction coefficients, which might be attributed to the fabrication without surfactants. The friction coefficients increase with the increase of Al_2O_3 coverage of the particles accordingly. Higher coverage corresponds to the higher friction coefficients. This result might be caused by the Al_2O_3 on the particles. The Al_2O_3 might be involved in friction behavior and lead to an increase in the friction coefficient.

3.4. Wear

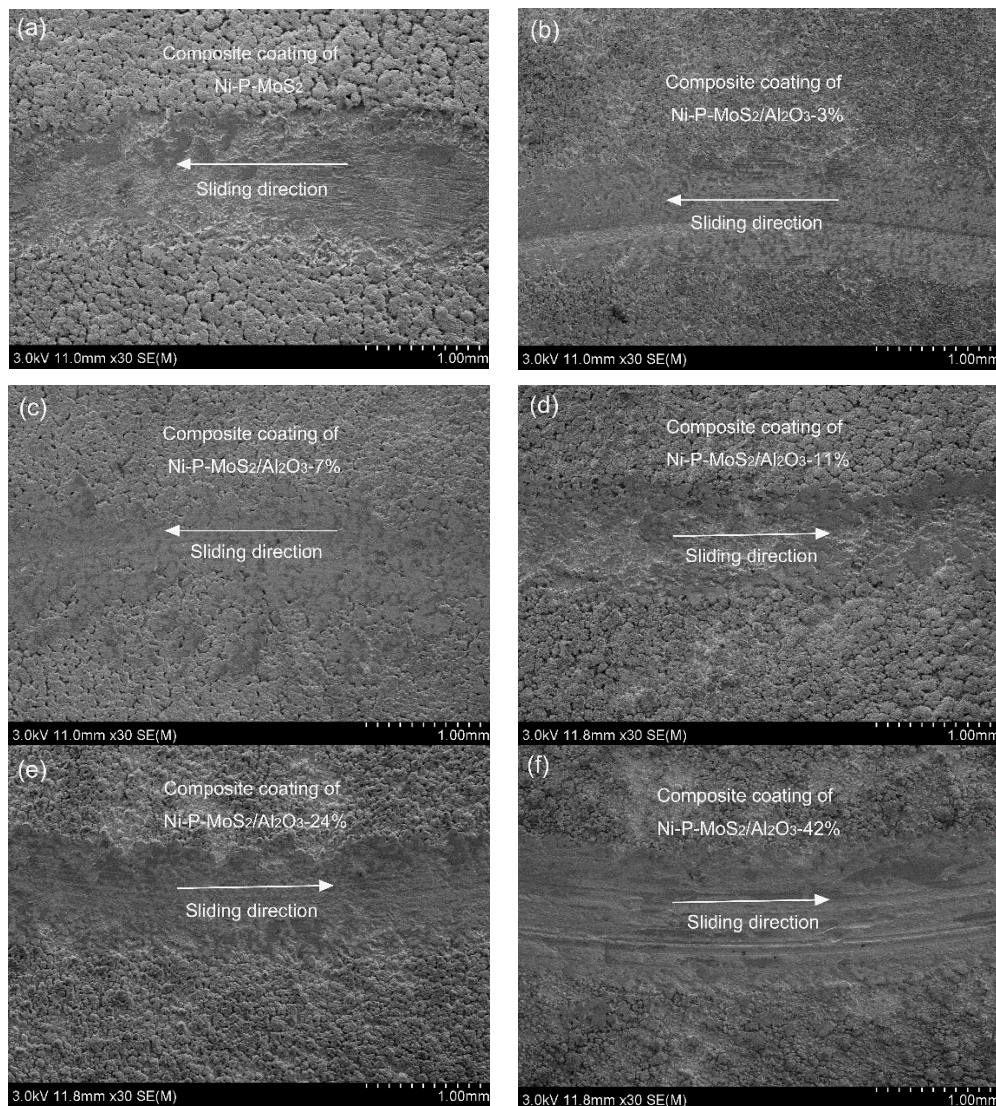Figure 8 demonstrates the mass loss of EN composite coatings incorporating Al_2O_3-coated MoS_2 particles with various coverage after wear. The mass loss of Ni–P–MoS_2 composite coating, about 0.63 mg/km, is lower than that of the Ni–P coating, which is approximately 0.70 mg/km. The less mass loss might be resulted from its remarkably decreased friction coefficient. Compared with Ni–P$\neq MoS_2$ composite coating, the composite coatings containing the coated MoS_2 with the coverage of 3% and 7% show a further reduction in mass loss in the range of 0.52–0.54 mg/km. The result could mainly be attributed to their fine and compact structures, which avoid the side-effects of surfactants. However, the composite coatings with higher coverage of MoS_2 show very large mass loss. The one with the coverage of 42% can reach 0.73 mg/km, exceeding the Ni–P alloy. The reason is mainly because it has a deteriorated surface structure and results in weak wear resistance.

Figure 8. Mass loss of EN composite coatings incorporating Al_2O_3-coated MoS_2 particles with various coverage.

Figure 9 presents SEM of the worn tracks for the composite coatings incorporating the coated MoS_2 with various coverage. The Ni–P–MoS_2 composite coating shows a rough worn surface with more ploughing and scuffing tracks. This is attributed to its relatively coarse structure, which provides severe wear and thus leads to an increasing friction coefficient when against the hard pair of WC materials, as shown in Figure 7. Both the composite coatings with the coverages of 3% and 7% show a relatively smooth and flat worn surface without obvious ploughing tracks. The results are in accordance with their respective steady evolution of the friction coefficient, and are mainly attributed to their respective fine and compact microstructures. However, the composite coatings containing MoS_2 with higher coverage of Al_2O_3 indicate a remarkably rough worn surface with numerous fine and closed-packed scuffing tracks. One main reason is that the loose coating structure has a lower bearing capacity for shear load during the sliding test. The other reason is that the free Al_2O_3 stripping from the surface of MoS_2 could turn into abrasive particles and accordingly intensify the interface destruction of both parts. As a result, these composite coatings show higher friction coefficients and worse wear resistance.

Figure 9. Worn track profile of electroless composite coatings incorporating Al_2O_3-coated MoS_2 particles with various coverages of (**a**) 0%, (**b**) 3%, (**c**) 7%, (**d**) 11%, (**e**) 24%, (**f**) 42%, respectively.

Figure 10 reveals the worn scar of the WC counter after sliding against the electroless Ni–P coating and the composite coatings containing MoS_2 with various coverage of Al_2O_3. The worn scar sliding against Ni–P coating shows a small and regular area with numerous ploughing tracks. Due to the MoS_2 lubricant, the worn scar sliding against Ni–P–MoS_2 composite coating is relatively smooth. A similar result is shown on the surface of counter-sliding against the composite coating with 3% coverage MoS_2 as well, which indicates the lesser coverage of Al_2O_3 does not change the lubricant property of MoS_2. When the coverage is up to 7%, the corresponding worn scar of the counter appears to be slightly rough. The further increase of the coverage of Al_2O_3 on MoS_2 would lead to a rougher worn surface on the counter, sliding against them. The numerous scuffing tracks on the worn scars can be seen. Apart from the loose surface of the composite coating, the stripping free Al_2O_3 from MoS_2 particles might be another reason for the deterioration of the worn surface.
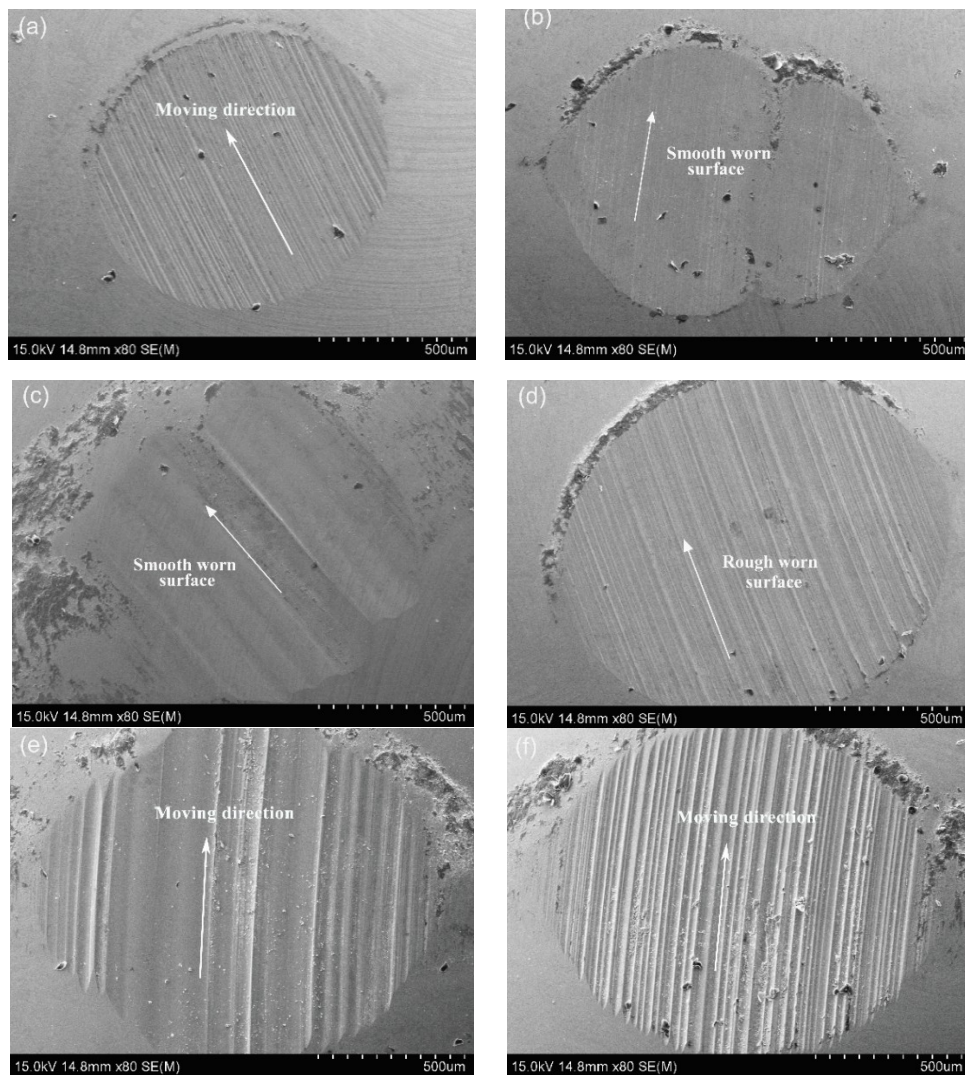
Figure 10. The worn scars of the WC counter after sliding against (**a**) EN, and its composite coatings incorporating Al_2O_3-coated MoS_2 particles with coverage of (**b**) 0%, (**c**) 3%, (**d**) 7%, (**e**) 24%, (**f**) 42%.

4. Conclusions

The Al_2O_3-coated MoS_2 particles with various coverages were obtained by using the heterogeneous nucleation process. The composite coatings with the coated particles were fabricated successfully in the absence of surfactants. The Al_2O_3 loading on MoS_2 particles shows significant influence on the friction and wear performance of composite coatings under dry sliding configuration. The composite coatings containing MoS_2 with lower Al_2O_3 loading show a fine roughness and compact structure, and thus correspond to higher wear resistance. Those containing MoS_2 with higher Al_2O_3 loading show a loose structure, and have less wear resistance. This study reveals that up to 7% Al_2O_3 coverage can achieve a quality composite coating without using surfactants. The small amount of Al_2O_3 offers the advantage of affecting the lubricant nature of MoS_2 particles much less, which in turn improves the wear property of the composite coating.

Author Contributions: Conceptualization, Y.Z.; Methodology, G.Z.; Formal Analysis, Z.H. and X.Z.; Investigation, M.J. and Q.S.; Writing, P.L.; Review and Editing, S.W. and S.Y.

Conflicts of Interest: The authors declare no conflict of interest.

References

1. Makkar, P.; Mishra, D.D.; Agarwala, R.C.; Agarwala, V. A novel electroless plating of Ni–P–Al–ZrO$_2$ nanocomposite coatings and their properties. *Ceram. Int.* **2014**, *40*, 12013–12021. [CrossRef]

2. Ardakani, S.R.; Afshar, A.; Sadreddini, S.; Ghanbari, A.A. Characterization of Ni–P–SiO$_2$–Al$_2$O$_3$ nano-composite coatings on aluminum substrate. *Mater. Chem. Phys.* **2017**, *189*, 207–214. [CrossRef]

3. Wu, H.; Liu, F.; Gong, W.; Ye, F.; Hao, L.; Jiang, J.; Han, S. Preparation of Ni–P–GO composite coatings and its mechanical properties. *Surf. Coat. Technol.* **2015**, *272*, 25–32. [CrossRef]

4. Novak, M.; Vojtech, D.; Vitu, T. Influence of heat treatment on tribological properties of electroless Ni–P and Ni-P-Al$_2$O$_3$ coatings on Al-Si casting alloy. *Appl. Surf. Sci.* **2010**, *256*, 2956–2960. [CrossRef]

5. Rahimi, A.R.; Modarress, H.; Iranagh, S.A. Effect of alumina nanoparticles as nanocomposites on morphology and corrosion resistance of electroless Ni–P coatings. *Surf. Eng.* **2011**, *27*, 26–31. [CrossRef]

6. Wang, Q.; Callisti, M.; Greer, J.; McKay, B.; Milickovic, T.K.; Zoikis-Karathanasis, A.; Deligkiozi, I.; Polcar, T. Effect of annealing temperature on microstructure, mechanical and tribological properties of nano-SiC reinforced Ni–P coatings. *Wear* **2016**, *356*, 86–93. [CrossRef]

7. Soleimani, R.; Mahboubi, F.; Kazemi, M.; Arman, S.Y. Corrosion and tribological behavior of electroless Ni–P/nano–SiC composite coating on aluminium 6061. *Surf. Eng.* **2015**, *31*, 714–721. [CrossRef]

8. Sadeghzadeh-Attar, A.; AyubiKia, G.; Ehteshamzadeh, M. Improvement in tribological behavior of novel sol-enhanced electroless Ni–P–SiO$_2$ nanocomposite coatings. *Surf. Coat. Technol.* **2016**, *306*, 837–848. [CrossRef]

9. Hosseini, J.; Bodaghi, A. Corrosion behaviour of electroless Ni–P–TiO$_2$ nanocomposite coatings using Taguchi. *Surf. Eng.* **2013**, *29*, 183–189. [CrossRef]

10. Reddy, V.; Ramamoorthy, B.; Nair, P. A study on the wear resistance of electroless Ni-P/Diamond composite coatings. *Wear* **2000**, *239*, 111–116. [CrossRef]

11. Li, Z.; Wang, J.; Lu, J.; Meng, J. Tribological characteristics of electroless Ni–P–MoS$_2$ composite coatings at elevated temperatures. *Appl. Surf. Sci.* **2013**, *264*, 516–521. [CrossRef]

12. Hu, X.; Jiang, P.; Wan, J.; Xu, Y.; Sun, X. Study of corrosion and friction reduction of electroless N–P coating with molybdenum disulfide nanoparticles. *J. Coat. Technol. Res.* **2009**, *6*, 275–281. [CrossRef]

13. Srinivasan, K.N.; John, S. Studies on electroless nickel–PTFE composite coatings. *Surf. Eng.* **2005**, *21*, 156–160. [CrossRef]

14. Hsua, C.I.; Hou, K.H.; Ger, M.D.; Wang, G.L. The effect of incorporated self-lubricated BN(h) particles on the tribological properties of Ni–P–BN(h) composite coatings. *Appl. Surf. Sci.* **2015**, *357*, 1727–1735. [CrossRef]

15. De Hazan, Y.; Knies, F.; Burnat, D.; Graule, T.; Yamada-Pittini, Y.; Aneziris, C.; Kraak, M. Homogeneous functional Ni–P/ceramic nanocomposite coatings via stable dispersions in electroless nickel electrolytes. *J. Colloid Interface Sci.* **2012**, *365*, 163–171. [CrossRef] [PubMed]

16. Sharma, A.; Singh, A.K. Electroless Ni–P–PTFE-Al$_2$O$_3$ dispersion nanocomposite coating for corrosion and wear resistance. *J. Mater. Eng. Perform.* **2014**, *23*, 142–151. [CrossRef]

17. Islama, M.; RizwanAzhar, M.; Fredj, N.; Burleigh, T.D.; Oloyede, O.R.; Almajid, A.A.; Shah, S.I. Influence of SiO$_2$ nanoparticles on hardness and corrosion resistance of electroless Ni–P coatings. *Surf. Coat. Technol.* **2015**, *261*, 141–148. [CrossRef]

18. Gadharia, P.; Sahoo, P. Optimization of Coating Process Parameters to Improve microhardness of Ni–P–TiO$_2$ composite coatings. *Mater. Today Proc.* **2015**, *2*, 2367–2374. [CrossRef]

19. Chen, Y.; Hao, Y.; Huang, W. Corrosion behavior of Ni–P–nano–Al$_2$O$_3$ composite coating in the presence of anionic and cationic surfactants. *Surf. Coat. Technol.* **2017**, *310*, 122–128. [CrossRef]

20. Tamilarasan, T.; Rajendran, R.; Rajagopal, G.; Sudagar, J. Effect of surfactants on the coating properties and corrosion behaviour of Ni–P–nano–TiO$_2$ coatings. *Surf. Coat. Technol.* **2015**, *276*, 320–326. [CrossRef]

21. Afroukhteh, S.; Dehghaniann, C.; Emamy, M. Preparation of electroless Ni–P composite coatings containing nano-scattered alumina in presence of polymeric surfactant. *Prog. Nat. Sci. Mater. Int.* **2012**, *22*, 318–325. [CrossRef]

22. Nwosu, N.; Davidson, A.; Hindle, C.; Barker, M. On the Influence of surfactant incorporation during electroless nickel plating. *Ind. Eng. Chem. Res.* **2012**, *51*, 5635–5644. [CrossRef]

23. Sudagar, J.; Lian, J.; Sha, W. Electroless nickel, alloy, composite and nano coatings—A critical review. *J. Alloy. Compd.* **2013**, *571*, 183–204. [CrossRef]

24. Agarwala, R.C.; Agarwala, V. Electroless alloy/composite coatings: A review. *Sadhana* **2003**, *28*, 475–493. [CrossRef]

25. Sudagar, J.; Lian, J.S.; Jiang, Q.; Jiang, Z.H.; Li, G.Y.; Elansezhian, R. The performance of surfactant on the surface characteristics of electroless nickel coating on magnesium alloy. *Prog. Org. Coat.* **2012**, *74*, 788–793. [CrossRef]

26. Zielinska, K.; Stankiewicz, A.; Szczygie, I. Electroless deposition of Ni–P–nano–ZrO$_2$ composite coatings in the presence of various types of surfactants. *J. Colloid Interface Sci.* **2012**, *377*, 362–367. [CrossRef] [PubMed]

27. Der Ger, M.; Hwang, B.J. Effect of surfactants on codeposition of PTFE particles with electroless Ni–P coating. *Mater. Chem. Phys.* **2002**, *76*, 38–45. [CrossRef]

28. Mafi, I.R.; Dehghanian, C. Comparison of the coating properties and corrosion rates in electroless Ni–P–PTFE composites prepared by different types of surfactants. *Appl. Surf. Sci.* **2011**, *257*, 8653–8658. [CrossRef]

29. Chen, B.H.; Hong, L.; Ma, Y.; Ko, T.M. Effects of Surfactants in an Electroless Nickel–Plating Bath on the Properties of Ni–P Alloy Deposits. *Ind. Eng. Chem. Res.* **2002**, *41*, 2668–2678. [CrossRef]

30. Amell, A.; Muller, C.; Sarret, M. Influence of fluoro surfactants on the codeposition of ceramic nanoparticles and the morphology of electroless Ni–P coatings. *Surf. Coat. Technol.* **2010**, *205*, 356–362. [CrossRef]

31. Nwosu, N.O.; Davidson, A.M.; Hindle, C.S. Effect of Sodium Dodecyl Sulphate on the Composition of Electroless Nickel-Yttria Stabilized Zirconia Coatings. *Adv. Chem. Eng. Sci.* **2011**, *1*, 118–124. [CrossRef]

32. Mai, Y.; Zhou, M.; Ling, H.; Chen, F.; Lian, W.; Jie, X. Surfactant-free electrodeposition of reduced graphene oxide/copper composite coatings with enhanced wear resistance. *Appl. Surf. Sci.* **2018**, *433*, 232–239. [CrossRef]

33. Abdoli, M.; Sabour Rouhaghdam, A. Preparation and characterization of Ni–P/nanodiamond coatings: Effects of surfactants. *Diam. Relat. Mater.* **2013**, *31*, 30–37. [CrossRef]

34. Zarebidaki, A.; Allahkaram, S.R. Effect of surfactant on the fabrication and characterization of Ni–P–CNT composite coatings. *J. Alloy. Compd.* **2011**, *509*, 1836–1840. [CrossRef]

35. Bulasara, V.K.; Babu, C.S.N.M.; Uppaluri, R. Effect of surfactants on performance of electroless plating baths for nickel-ceramic composite membrane fabrication. *Surf. Eng.* **2012**, *28*, 44–48. [CrossRef]

36. Tamilarasan, T.R.; Rajendran, R.; Sivashankar, M.; Sanjith, U.; Rajagopal, G.; Sudagar, J. Wear and scratch behaviour of electroless Ni-P-nano-TiO$_2$: Effect of surfactants. *Wear* **2016**, *346*, 148–157. [CrossRef]

37. Song, X.; Jiang, N.; Li, Y.; Xu, D.; Qiu, G. Synthesis of CeO$_2$-coated SiO$_2$ nanoparticle and dispersion stability of its suspension. *Mater. Chem. Phys.* **2008**, 128–135. [CrossRef]

38. Zuo, D.; Tian, G.; Li, X.; Chen, D.; Shu, K. Recent progress in surface coating of cathode materials for lithium ion secondary batteries. *J. Alloy. Compd.* **2017**, *706*, 24–40. [CrossRef]

39. Zuo, D.; Tian, G.; Chen, D.; Shen, H.; Lv, C.; Shu, K.; Zhou, Y. Comparative study of Al$_2$O$_3$-coated LiCoO$_2$ electrode derived from different Al precursors uniformity, microstructure and electrochemical properties. *Electrochim. Acta* **2015**, *178*, 447–457. [CrossRef]

40. Liu, P.; Zhu, Y.; Zhang, S. Hydrophilicity characterization of Al$_2$O$_3$-coated MoS$_2$ particles by using thin layer wicking and sessile drop method. *Powder Technol.* **2015**, *281*, 83–90. [CrossRef]

41. Liu, Y.; Zhu, Y.; Liu, P.; Liu, T. Surface coating and application in plating of MoS$_2$ powders with Al$_2$O$_3$. *China Surf. Eng.* **2012**, *25*, 97–102. (In Chinese)

42. Liu, T.; Zhu, Y.; Liu, Y.; Zhang, S. Preparation and properties of Ni–P–MoS$_2$/Al$_2$O$_3$ composite coating. *Lubr. Eng.* **2013**, *38*, 46–50. (In Chinese)

43. Liu, Y.F.; Zhu, Y.W.; Liu, T.T.; Zhang, S.W.; Peng, Y. Friction and wear properties of Ni–P electroless composite coatings with core-shell nanodiamond. *Tribology* **2013**, *33*, 267–274.

44. Gan, B.K.; Madsen, I.C.; Hockridge, J.G. In situ X-ray diffraction of the transformation of gibbsite to a-alumina through calcination: Effect of particle size and heating rate. *J. Appl. Crystallogr.* **2009**, *42*, 697–705. [CrossRef]

45. Bigdeli, F.; Allahkaram, S.R. An investigation on corrosion resistance of asapplied and heat treated Ni–P/nanoSiC coatings. *Mater. Des.* **2009**, *30*, 4450–4453. [CrossRef]

46. Apachitei, I.; Tichelaar, F.D.; Duszczyk, J.; Katgerman, L. The effect of heat treatment on the structure and abrasive wear resistance of autocatalytic NiP and NiP–SiC coatings. *Surf. Coat. Technol.* **2002**, *149*, 263–278. [CrossRef]

47. Hu, X.G.; Cai, W.J.; Xu, Y.F.; Wan, J.C.; Sun, X.J. Electroless Ni–P–(nano-MoS$_2$) composite coatings and their corrosion properties. *Surf. Eng.* **2009**, *25*, 361–366. [CrossRef]

48. Elansezhian, R.; Ramamoorthy, B.; Nair, P.K. The influence of SDS and CTAB surfactants on the surface morphology and surface topography of electroless Ni–P deposits. *J. Mater. Proc. Technol.* **2009**, *209*, 233–240. [CrossRef]

49. Moonir-Vaghefi, S.M.; Saatchi, A.; Hejazi, J. Deposition and properties of electroless nickel–phosphorus–molybdenum disulfide composites. *Met. Finish.* **1997**, *95*, 46, 48, 50–52. [CrossRef]